Brief Review

Modern Physics Letters B, Vol. 20, Nos. 2 & 3 (2006) 63–95

World Scientific
www.worldscientific.com

LOCALIZATION AND GLASSY DYNAMICS IN THE IMMUNE SYSTEM

JUN SUN, DAVID J. EARL and MICHAEL W. DEEM

Department of Bioengineering and Department of Physics & Astronomy, Rice University, Houston, TX 77005–1892, USA

Received 3 October 2005

We discuss use of the generalized NK model to examine evolutionary dynamics within the immune system. We describe how randomness and diversity play key roles in the immune response and how their effects are captured by this hierarchical spin glass model. We discuss analytical aspects of the model as well as practical applications to design of the annual influenza vaccine. We discuss the subtle role that the glassy evolutionary dynamics plays in suppressing autoimmune disease.

Keywords: Immune system; protein evolution; spin glass; cross-reactivity.

PACS Number(s): 87.10.+e, 87.15.Aa, 87.17.-d, 87.23.Kg

1. Introduction

The immune system provides a biological example of a random and evolving system. A successful description of the immune system must capture several essential biological features. First, each person has only a finite number of antibodies, out of a very large space of possible antibodies. Second, dynamics are important, because diseases must be cleared from an infected person by the immune system in a finite time. Third, there are correlations between the immune system and the infection, because diseases evolve in response to immune system pressure. Due to these technical features, the immune system is a natural object for study by statistical mechanics.

The immune system is not completely understood, and new scientific discoveries can have significant impacts on public health. For example, the annual mortality due to influenza epidemics is 250000 to 500000 people worldwide, and 5 to 15% of the total population becomes ill each year.[1] Typical annual costs associated with influenza outbreaks in the U.S. are $10 billion,[2] with approximately 40000 deaths, but this figure rises to around 90000 if individuals with susceptible complications are included.[3,4] The economic cost of an influenza pandemic is estimated to be between $71–167 billion in the USA alone.[5] Vaccination is the primary public health method used to prevent infection with high death rate in the population.[6]

The development of quantitative models of the performance of the immune system response to highly variable viral diseases is an area ripe for investigation. Of the 14 "Grand Challenges in Global Health," six Grand Challenges are vaccine related, and two Grand Challenges are addressed by such quantitative models.[7] Over the past 35 years, the average efficacy of the influenza vaccine has been about 42% of what it could be for a perfectly designed vaccine, both due to the mutation of the flu and to the less than optimal design of the vaccine.[8] The flu shot has even had a negative efficacy 26% of the time.[8] Two of the most well-known diseases with high death rates, cancer and HIV, are immunity related, and both raise challenges to vaccine design due to their high mutation rates and diversities. Autoimmunity, i.e. when an immune response is mistakenly directed at a person's own proteins, is a poorly understood aspect of immunology that is growing in practical importance. Autoimmune diseases affect some 50 million Americans, are one of the top ten leading causes of death in children and women aged 65 years and younger, and cost nearly $100 billion every year in direct health care in the U.S.[9]

The antibodies of the immune system evolve during an immune response. This evolution occurs in the sequence space of the antibodies that recognize the disease. The free energy of binding between an antibody and an invading pathogen depends in a rugged and somewhat unpredictable way on the amino acid sequence. We, therefore, expect evolution of antibodies to be generically slow and perhaps glassy. Thus, we are motivated to model the protein evolution that occurs in the immune response with dynamics on a spin glass model.[10] The energy landscapes of our model proteins, as a function of amino acid sequence space, are quite rugged. Protein folding occurs on a much more rapid timescale than the evolutionary dynamics that we consider. Thus, we focus on the the amino acid sequence degrees of freedom.

Our work complements the traditional literature of mean-field, differential equation based approaches to the immune system by allowing an investigation of the sequence-level dynamics of the finite size immune system. The antibodies produced in response to an antigen, and whether these same antibodies clear the disease or might cause autoimmune disease, are of our interest. The dynamics of the immune response, variable diversity joining (VDJ) recombination and somatic hypermutation, are captured by the mutation and selection dynamics of our model. Exactly these evolutionary dynamics are what our model can capture, and what differential equation based models cannot. That is, the sequence based approach we describe captures the diversity of the immune system, which is not intrinsically included in mean field theories.

The hierarchical structure of proteins induces a hierarchical structure to the ruggedness of the amino acid sequence space in which antibodies evolve. That is, depending on the dynamics and mechanisms used to search sequence space, energy barriers of different magnitude are crossed and these barriers are correlated in a hierarchical way. To describe the biology properly, it is essential to take into account this hierarchical nature of the evolution. Hierarchy is a novel feature of the spin glass model we will discuss. In nature there exists a wide range of evolutionary

mechanisms,[11−14] which range from point mutation to recombination to swapping events, and this hierarchy is exploited in evolution in the immune system as well.[15] One set of evolutionary moves has evolved to provide initial starting sequences for antibodies, VDJ recombination, and another set of evolutionary moves has evolved to fine tune these sequences, somatic hypermutation.

The rest of this paper is organized as follows. In Sec. 2, we provide a brief description of the immune system. In Sec. 3, we describe the sequence-based, hierarchical spin glass model that we use to describe antibody evolution in the immune system. We also present some of the analytic properties of this model. In Sec. 4, we describe the phenomenon and mechanism of original antigenic sin. In Sec. 5, we describe a new order parameter derived from the theory that correlates well with efficacy of the annual flu shot. In Sec. 6, we describe how the glassy nature of evolution within the immune system helps to avoid autoimmune disease. We conclude in Sec. 7. Shorter versions of some of these results have appeared previously.[8,16,17]

2. Brief Description of the Immune System

The immune system protects our body against infection from invading pathogens. The immune system is composed of cells and molecules circulating in the fluid of our tissues that interact with each other through signaling and act together to locate and eliminate invaders. The immune system is classified into two subsystems, the innate and the adaptive immune system. The former recognizes invading foreign bodies using a general mechanism, whereas the latter recognizes pathogens in a specific way. The adaptive immune response is further divided into two categories, namely the humoral, or B cell, response and the cellular, or T cell, response. The humoral immune response, which is dedicated to the elimination of extracellular pathogens, is the focus of this paper.

The main function of the humoral immune response is to develop B cells that produce antigen specific antibodies. An antibody molecule consists of two identical heavy and two identical light protein chains. When a B cell produces an antibody that binds to an antigen specifically, it begins to divide. This division occurs in one of the many lymph nodes of the body and occurs several times per day.

The diversity of the antibody molecules originates from a process called VDJ recombination, in which gene fragments randomly selected from three different genetic pools (V, D, and J) in the genome are joined together to create a set of initial antibodies. This process can produce on the order of 10^{12} to 10^{14} different antibodies from one genome.[15] Those B cells that produce antibodies that recognize an invading pathogen undergo a second evolutionary process of somatic hypermutation. In this process, the B cells that produce antibodies which bind to the antigen with higher affinities are selected and expanded in number by division. During this process, the DNA that codes for the antibody binding region is also mutated. For this reason, this second evolutionary process is called somatic hypermutation. Somatic hypermutation essentially performs a local search in the amino acid sequence

space at the level of individual point mutations for higher affinity, starting from the initial VDJ starting points.[18] Somatic hypermutation can be viewed as a local diffusion in the antibody sequence space.

The process of antibody binding to antigen is a reversible chemical reaction:

$$K^{\mathrm{eq}} = \frac{[\mathrm{Antibody} : \mathrm{Antigen}]}{[\mathrm{Antibody}][\mathrm{Antigen}]}\,, \tag{1}$$

where $[\cdot]$ is the concentration, and the binding constant K ranges from 10^4 to 10^{11} l/mol in experimental studies of antibody-antigen binding.[15,19]

Following somatic hypermutation, some B cells differentiate into plasma cells and others become memory cells. Plasma cells secrete soluble effector antibodies that bind antigen and block them from entering cells, mark antigen and signal phagocytic cells to ingest and destroy the invaders, or activate complement and punch holes in the membranes of the pathogen. Memory cells will stay longer at peripheral areas, such as lymph nodes, with membrane-bound antibody having the same specificity as the effector antibodies. Normally, memory cells help the immune system to mount a more effective response if the host is exposed to a pathogen that is very similar to the one previously encountered. The memory mechanism is also the foundation for vaccination. The vaccine is a first exposure and causes the production of memory cells that are prepared for a more effective response upon subsequent exposure.

3. Hierarchical Spin Glass Model of Antibody Evolution

We use a hierarchical spin glass model to represent the folding of antibodies and the interactions between antibodies and antigen.[16,20] The model captures the correlated ruggedness of the interaction energy in the variable space provided by the antibody amino acid sequences and the identity of the antigen, with the correlations being mainly due to the physical structure of the antibodies. The hierarchical structure also distinguishes our model from traditional short- or long-range spin glass energy models.[21,22] Our model allows study of the sequence-level dynamics of the immune/antigen system, which would otherwise be an intractable problem at the atomic scale, with 10^4 atoms per antibody, 10^8 antibodies per individual, 6×10^9 individuals, and many possible disease strains. Use of random energy theory to treat correlations in otherwise intractable physical systems goes back at least to Bohr's random matrix theory for nuclear cross sections[23] and has been used for quantum chaos, disordered mesoscopic systems, QCD, and quantum gravity.[24] Spin glass models were first introduced in the context of dilute magnetic ions randomly distributed in a nonmagnetic alloy.[25–27] The "frustration effect" in spin glass models makes the dynamics and equilibrated properties nontrivial and endows these models with fundamental physical importance.[28] Spin glass models have been applied in biology to simulate RNA evolution, to explain the origin of biological systems, and to study protein-folding and function.[10,29–33] Spin glass models have been used to capture the random interactions that occur between biological agents. Spin glass

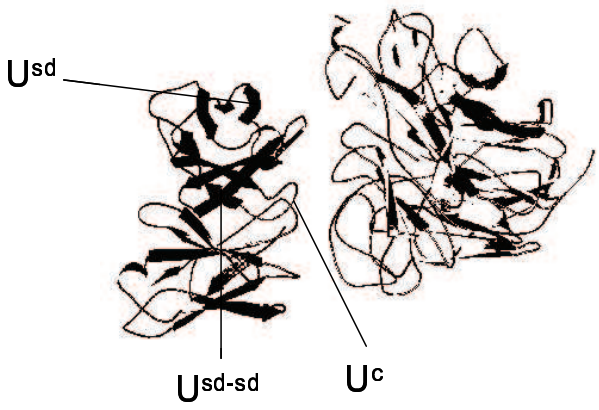

Fig. 1. The binding of an antibody to an antigen is drawn. The antigen is on the right and the antibody is on the left. The interactions within a subdomain (U^{sd}), interactions between subdomains ($U^{\mathrm{sd-sd}}$), and direct binding interactions between an antibody and an antigen (U^{c}) are shown. Different antibodies recognize and fold in response to different antigens; therefore the corresponding U^{sd}, $U^{\mathrm{sd-sd}}$ and U^{c} will change.

Table 1. Parameters and values for the generalized NK model.

Parameter	Value	Definition
K	4	Local interaction range within a subdomain
M	10	Number of secondary structure subdomains
N	10	Number of amino acids in each subdomain
P	5	Number of amino acids contributing directly to the binding
L	5	Number of subdomain types (e.g., helices, strands, loops, turns and others)
a_j		Identity of amino acid at sequence position j
α_i	$1 \leq \alpha_i \leq L$	Type of secondary structure for the ith subdomain
σ_{α_i}		Local interaction coupling within a subdomain, for subdomain type α_i
D	6	Number of interactions between subdomains
σ_{ij}^{k}		Nonlocal interaction coupling between secondary structures
σ_i		The ith direct coupling between antibody and antigen

models have been used to study population- and sequence-level dynamics of biological systems, capturing the many different local minima available at the same energy level in sequence space, and allowing study of topics such as the diversity, stability, and evolvability of biological systems.[13,34] Close to the present application is the study of spin glasses by random energy models,[26,27] protein folding by coarse-grained models,[30,31] and evolutionary systems by NK-type models.[20,32,35,36]

In detail, the generalized NK model we use, as shown in Fig. 1, considers three different kinds of interactions within an antibody: interactions within a subdomain (U^{sd}), interactions between subdomains ($U^{\mathrm{sd-sd}}$), and direct binding interactions

between an antibody and an antigen (U^{c}). In the context of protein evolution, the parameters of the model have been calibrated.[16,20,33,37,38] We also list all the parameters and their values in Table 1. The energy function of a protein is given by

$$U = \sum_{i=1}^{M} U_{\alpha_i}^{\mathrm{sd}} + \sum_{i>j=1}^{M} U_{ij}^{\mathrm{sd-sd}} + \sum_{i=1}^{P} U_i^{\mathrm{c}}\,, \tag{2}$$

where M is the number of antibody secondary structural subdomains, and P is the number of amino acids in the antibody contributing directly to the binding. The subdomain energy U^{sd} is

$$U_{\alpha_i}^{\mathrm{sd}} = \frac{1}{\sqrt{M(N-K+1)}} \sum_{j=1}^{N-K+1} \sigma_{\alpha_i}(a_j, a_{j+1}, \ldots, a_{j+K-1})\,, \tag{3}$$

where N is the number of amino acids in a subdomain, and $K = 4$ specifies the range of local interactions within a subdomain. The subdomain is a cluster of amino acids encoded by a gene segment. There are interactions between the neighboring amino acids and $U_{\alpha_i}^{\mathrm{sd}}$ captures these interactions within all the subdomains. This value of K was initially fit by phenomenological comparison to phage display experiments.[38] We note that the helical period is 3.7 amino acids in an α helix, which is another reason for a local interaction range of $K = 4$. All subdomains belong to one of $L = 5$ different types (e.g., helices, strands, loops, turns, and others). The quenched Gaussian random number σ_{α_i} is different for each value of its argument for a given subdomain type, α_i. We consider only five chemically distinct amino acid classes[39] (e.g., negative, positive, polar, hydrophobic, and other) since each different type of amino acid behaves as a completely different chemical entity within the random energy model. So, the arguments a_j could be any number between 1 and 5 depending on their classes. All of the Gaussian σ values have zero mean and unit variance. The energy of interaction between secondary structures is

$$U_{ij}^{\mathrm{sd-sd}} = \sqrt{\frac{2}{DM(M-1)}} \sum_{k=1}^{D} \sigma_{ij}^{k}(a_{j_1}^{i}, \ldots, a_{j_{K/2}}^{i};\ a_{j_{K/2+1}}^{j}, \ldots, a_{j_K}^{j})\,. \tag{4}$$

We set the number of interactions between secondary structures at $D = 6$. $U_{ij}^{\mathrm{sd-sd}}$ captures the non-local interactions between amino acids. The total number of interactions with a typical amino acid is roughly 12, and roughly half of these, $[2(K-1)]$, are in U^{sd}, and the other half, $[D(M-1)K/(2N)]$, are in $U^{\mathrm{sd-sd}}$. Here σ_{ij}^{k} and the interacting amino acids, $j_1, \ldots, j_K$, are selected at random for each interaction (k, i, j). The σ_{ij}^{k} is a quenched Gaussian random number with zero mean and unit variance. The chemical binding energy between an antibody amino acid and antigen is given by

$$U_i^{\mathrm{c}} = \sigma_i(a_i)/\sqrt{P}\,. \tag{5}$$

The contributing amino acid, i, and the unit-normal weight of the binding, σ_i, are chosen at random. Using experimental results, we take $P = 5$ amino acids to contribute directly to the binding event.

The generalized NK model, while a simplified description of real proteins, captures much of the thermodynamics of protein folding and ligand binding. In the model, a specific B cell repertoire is represented by a specific set of amino acid sequences. Moreover, a specific instance of the random parameters, i.e. set of σ values, within the model represents a specific antigen. Different antigens correspond to different sets of parameters. Two antigens that differ in sequence by fraction p correspond to two sets of parameters that differ by p as well. An immune response that finds a B cell that produces an antibody with a high affinity constant to a specific antigen corresponds in the model to finding a sequence having a low energy for a specific parameter set.

The random character of the generalized NK model makes the energy rugged in antibody sequence space. The energy, moreover, is correlated due to the local antibody structure (U^{sd}), the secondary antibody structure ($U^{\mathrm{sd-sd}}$), and the direct interaction with the antigen (U^{c}). As the immune system explores the space of possible antibodies, localization is possible if the correlated ruggedness of the interaction energy is sufficiently great.

Since the variable region in each light and heavy chain of an antibody is about 100 amino acids long, and since most of the binding occurs in the heavy chain, we choose a sequence length of 100 residues.[40,41] We choose $M = 10$ since there are roughly 10 secondary structures in a typical antibody and thus choose $N = 10$. The immune system contains of the order of 10^8 B cells divided into different specificities, and the frequency of a specific B cell participating in the initial immune response is roughly 1 in 10^5.[15] Hence, we use 10^3 sequences during an immune response.

The immune system employs a hierarchical strategy to search antibody sequence space for high affinity antibodies. In our model an initial combination of optimized subdomains, produced by VDJ recombination, is followed by a point mutation and selection procedure, somatic hypermutation.[16] The flow chart of the process is shown by the solid lines in Fig. 2. To mimic the combinatorial joining of gene segments that occurs during B cell development, we produce a naive B cell repertoire by choosing each subdomain sequence from pools that have N_{pool} amino acid segments obtained by minimizing U^{sd} for that type of secondary structure. To fit the theoretical heavy-chain diversity of 3×10^{11},[15] we choose $N_{\mathrm{pool}} = 3$ sequences among the top 300 sequences for each subdomain type, because $(N_{\mathrm{pool}} \times L)^M \cong 6 \times 10^{11}$.

We can deduce approximate lower bounds for each term in the generalized NK model, Eq. (2), immediately after the initial VDJ recombination. We first calculate the effective diversity or effective population size arising from each term. We define the effective population size to be the number of different energy values found for that term in the whole population of N_{size} sequences, which is the effective different sequences for that term. From the diversity we then calculate the bound on the term. For pedagogical reasons, we first examine the second term, $U^{\mathrm{sd-sd}}$. The term $U^{\mathrm{sd-sd}}$ varies when any of the subdomain sequences is replaced by a different sequence from the same type pool. This is because $U^{\mathrm{sd-sd}}$ couples to many amino acids in each subdomain, and so if even one amino acid changes, the value of this

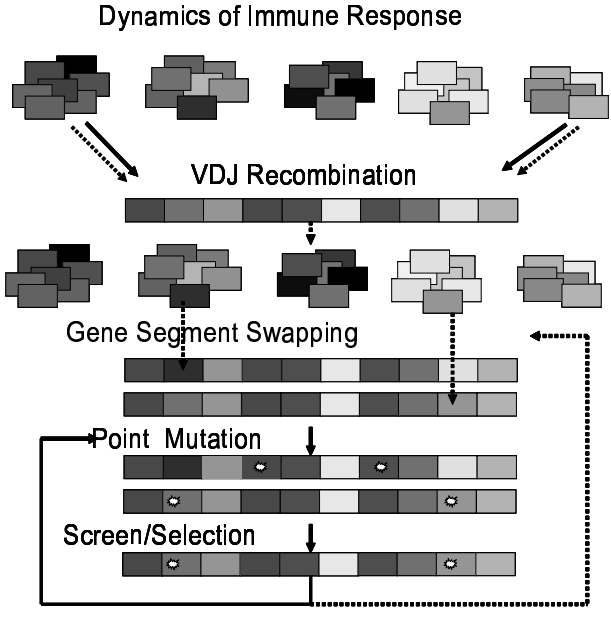

Fig. 2. The dynamics of the immune system in searching the sequence space for high affinity antibody is drawn. The flow described by solid lines is the dynamics used by the natural immune system. The flow represented by dashed lines is the dynamics that could be utilized by the immune system.

term changes. Given a set of parameters σ and the type of each subdomain in the sequence, $N_{\text{size}} = 1000$ sequences are sampled from the sequence space induced by VDJ recombination. For each subdomain, there are $N_{\text{pool}} = 3$ choices. We represent the sequence space that the VDJ recombination samples from by the states $\mathbf{s} = (s_1, s_2, \ldots, s_M)$, where $1 \leq s_i \leq 3$, and size of this space is $\Omega^{\text{sd}-\text{sd}} = 3^M$. All states are equally likely to be chosen. The placement of $N_{\text{size}} = 1000$ sequences in the state space is a Poisson process. So, the probability that n sequences occupy one particular state is

$$p(n) = p^n (1-p)^{N_{\text{size}}-n} \binom{N_{\text{size}}}{n}, \tag{6}$$

where $\binom{N_{\text{size}}}{n} = \frac{N_{\text{size}}!}{n!(N_{\text{size}}-n)!}$, and $p = \frac{1}{3^M}$. Therefore, the average effective population is

$$\langle N_{\text{eff}}^{\text{sd}-\text{sd}} \rangle = \sum_{\mathbf{s}} [1 - p(n=0)] = \Omega^{\text{sd}-\text{sd}} [1 - (1-p)^{N_{\text{size}}}]. \tag{7}$$

In Fig. 3, we show the dependence of the effective size on M. This result gives an essentially exact description for the effective diversity of $U^{\text{sd}-\text{sd}}$.

Now, we consider the effective population for the first term in Eq. (2), U^{sd}. The analysis is more involved in this case, because the space Ω^{sd} depends on the number of subdomains of type i, $\mathbf{n} = (n_1, \ldots, n_L)$, and on the number of times the

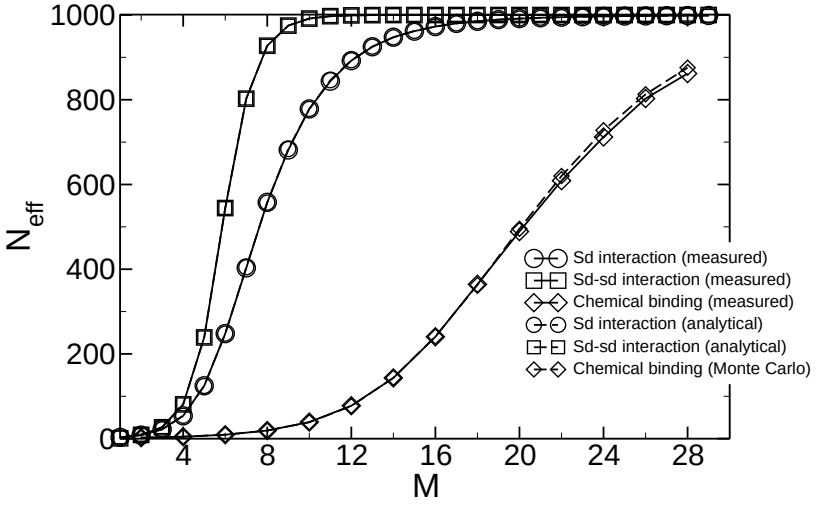

Fig. 3. The effective population size for the three terms in the generalized NK model, $\langle N_{\rm eff}^{\rm sd-sd}\rangle$, $\langle N_{\rm eff}^{\rm sd}\rangle$, and $\langle N_{\rm eff}^{\rm c}\rangle$. Also shown are the analytical results for $\langle N_{\rm eff}^{\rm sd-sd}\rangle$, $\langle N_{\rm eff}^{\rm sd}\rangle$. A Monte Carlo evaluation is shown for $\langle N_{\rm eff}^{\rm c}\rangle$.

jth subdomain is chosen from pool type i, s_i^j. We note $\sum_i n_i = M$, and $\sum_j s_i^j = n_i$. Because the sequences in the VDJ pools are unique, $U^{\rm sd}$ differs if any of the values of s_i^j is different. The effective population for a given value of $\mathbf{n}$ is of a form similar to that of Eq. (7). The average effective population is calculated by averaging over $\mathbf{n}$. Thus, the average effective population for $U^{\rm sd}$ is

$$\langle N_{\rm eff}^{\rm sd}\rangle = \sum_{\mathbf{n}} p(\mathbf{n}) \sum_{\mathbf{s}} \{1 - [1 - p(\mathbf{s}|\mathbf{n})]^{N_{\rm size}}\}\,, \tag{8}$$

where $p(\mathbf{n}) = \frac{M!}{L^M \prod_i n_i!}$ is the probability distribution for $\mathbf{n}$, and $p(\mathbf{s}|\mathbf{n}) = \prod_i \frac{n_i!}{3^{n_i} \prod_j s_i^j!}$ is the conditional probability distribution of $\mathbf{s}$ given the value of $\mathbf{n}$. The dependence of the effective size of $U^{\rm sd}$ on M is shown in Fig. 3. Again, this result gives an essentially exact description for the effective diversity of $U^{\rm sd}$.

Finally, we calculate the effective population size for $U^{\rm c}$. We note that the types of the M subdomains are chosen randomly from $L = 5$ types, defining $\mathbf{n} = (n_1, \ldots, n_L)$ with $\sum_i n_i = M$. Furthermore, the $P = \frac{M}{2}$ binding sites are randomly distributed among the M subdomains, defining $\mathbf{m} = (m_1, \ldots, m_M)$ with $\sum_j m_j = P$. The term $U^{\rm c}$ will differ when the amino acids chosen in a given subdomain differ among the $N_{\rm pool} = 3$ subdomains in the pool. We define the probability of diversity k at a given site to be p_k. Assuming that the amino acids in the pool are randomly distributed by the subdomain generation process, we find $p_1 = \frac{1}{Q^2}$, $p_2 = \frac{3(Q-1)}{Q^2}$, and $p_3 = \frac{(Q-1)(Q-2)}{Q^2}$, where $Q = 5$ is the number of distinct amino acid types. We let $D_{0,j}^i$, $i = 1, L$ and $j = 1, n_i$, be the diversity of the jth subdomain of type i. The diversity can be 1, 2, or 3. The diversity between different subdomains of the same

type in which some of the chosen binding sites are identical is correlated, because subdomains of a given type are chosen from the same pool. Nonetheless, given $\mathbf{n}$ and $\mathbf{m}$, one can evaluate the probability of the diversity of all subdomains, $p(\mathbf{D}_0|\mathbf{n},\mathbf{m})$, where $\mathbf{D}_0 = (D^1_{0,1},\ldots,D^1_{0,n_1};\ldots;D^L_{0,1},\ldots,D^L_{0,n_L})$, represents the diversity at each subdomain. The effective population for $U^{\rm c}$ is

$$\langle N^{\rm c}_{\rm eff}\rangle = \sum_{\mathbf{n}} p(\mathbf{n}) \sum_{\mathbf{m}} p(\mathbf{m}) \sum_{\mathbf{D}_0} p(\mathbf{D}_0|\mathbf{m},\mathbf{n}) \sum_{\mathbf{s}} \{1-[1-p(\mathbf{s}|\mathbf{D}_0)]^{N_{\rm size}}\}\,, \qquad (9)$$

where $p(\mathbf{n}) = \frac{M!}{L^M \prod_i n_i!}$, and $p(\mathbf{m}) = \frac{P!}{M^P \prod_j m_j!}$. The term $p(\mathbf{s}|\mathbf{D}_0)$ is the probability of choosing state $\mathbf{s} = (s_1,\ldots,s_M)$ out of the space $\mathbf{D}_0$. We note $p(\mathbf{s}|\mathbf{D}_0) = \prod_{i=1}^L p(\mathbf{s}_i|\mathbf{D}^i_0)$, where $\mathbf{D}^i_0$ is the diversity of the subdomains of type i. Here $s_i = 1,2,3$ represents, respectively, the 1st, 2nd, and 3rd sample subdomain in the pool of the ith subdomain in the sequence. One sees that $p(1|D^i_{0,j}=1) = 1$, $p(2|D^i_{0,j}=1) = 0$, $p(3|D^i_{0,j}=1) = 0$; $p(1|D^i_{0,j}=2) = \frac{2}{3}$, $p(2|D^i_{0,j}=2) = \frac{1}{3}$, $p(3|D^i_{0,j}=2) = 0$; and $p(1|D^i_{0,j}=3) = \frac{1}{3}$, $p(2|D^i_{0,j}=3) = \frac{1}{3}$, $p(3|D^I_{0,j}=3) = \frac{1}{3}$. We can evaluate $\langle N^{\rm c}_{\rm eff}\rangle$ in several ways. We can perform the summation in Eq. (9) exactly, although this requires evaluation of $p(\mathbf{D}_0|\mathbf{m},\mathbf{n})$ directly. Or, we can sample $p(\mathbf{D}_0|\mathbf{m},\mathbf{n})$ by Monte Carlo. This latter approach is the one we take. We generate subdomain pools where the amino acids at each position are independent, randomly define the types of each subdomain, and randomly choose each subdomain sequence from the pool. We then calculate the diversity, averaging over many instances of this random process, to give the data shown in Fig. 3. The deviation between Eq. (9) and the measured data at large M is due to correlations between the diversity of binding sites chosen at different positions in same or different subdomains of the same type. The diversity becomes more sensitive to these correlations at large M, because more binding sites are being assigned from the fixed $N_{\rm pool} = 3$ subdomains in the pools.

If we neglect the correlations that arise when the same amino acid position is chosen to be a binding site in different subdomains of the same type, then Eq. (9) can be reduced to

$$\langle N^{\rm c}_{\rm eff}\rangle = \sum_{\mathbf{m}} p(\mathbf{m}) \sum_{\mathbf{D}_0} p(\mathbf{D}_0|\mathbf{m}) \sum_{\mathbf{s}} [1-[1-p(\mathbf{s}|\mathbf{D}_0)]^{N_{\rm size}}]\,, \qquad (10)$$

where $\mathbf{m}$ and $\mathbf{s}$ are as defined in Eq. (9). $\mathbf{D}_0 = (D^1_{0,1},\ldots,D^1_{0,n_1};\ldots;D^L_{0,1},\ldots,D^L_{0,n_L})$ is formally the same as $\mathbf{D}_0$, but now $D^i_{0,j}$ are independent of each other. In this case, we find

$$\begin{aligned} p(D^i_{0,j}=1|m^i_j) &= p_1^{m^i_j} \\ p(D^i_{0,j}=2|m^i_j) &= \sum_{k=1}^{m^i_j} \left(\frac{1}{3}\right)^{k-1} p_2^k p_1^{m^i_j-k} \binom{m^i_j}{k} \\ p(D^i_{0,j}=3|m^i_j) &= 1 - p(D^i_{0,j}=1|m^i_j) - p(D^i_{0,j}=2|m^i_j)\,. \end{aligned} \qquad (11)$$

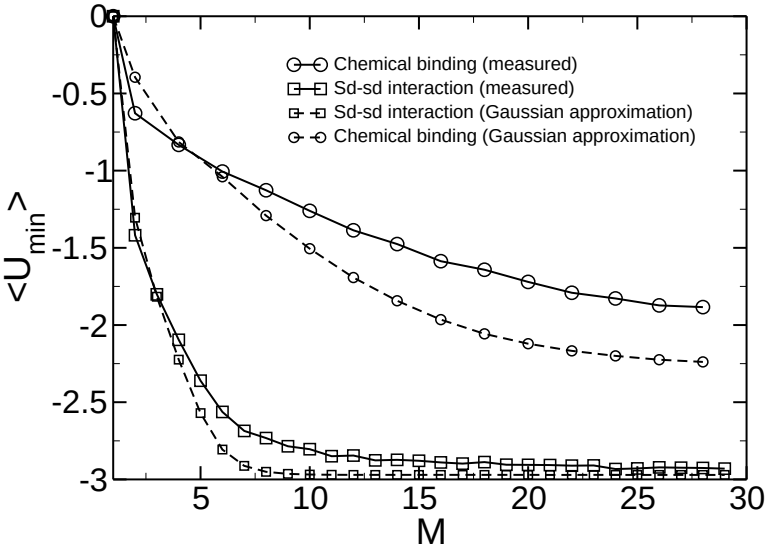

Fig. 4. The average minimum value of two terms in the generalized NK model, $\min U^{\mathrm{sd-sd}}$ and $\min U^{\mathrm{c}}$. Also shown are the analytical approximations for $\min U^{\mathrm{sd-sd}}$ and $\min U^{\mathrm{c}}$.

This result differs from Eq. (9) by less than 1% even at the largest values of M shown.

Now, we calculate approximate bounds for each energy term based on its effective population size. If we take the minimum of N independent identically distributed random numbers, x_i, each with probability distribution $p(x)$, we find

$$\langle \min(x_i; i = 1, N) \rangle = \int_{-\infty}^{\infty} xNp(x)p_{>}(x)^{N-1}dx\,, \tag{12}$$

where $p_{>}(x) = \int_x^{\infty} p(y)dy$. We assume that U^{sd}, $U^{\mathrm{sd-sd}}$, and U^{c} obey a Gaussian distribution and measure their variances in a given instance of the generalized NK ensemble.[a] Using the effective population sizes from Fig. 3 and the measured variances, we find lower bounds to each term immediately after VDJ recombination as $U^{\mathrm{sd}} = \langle U^{\mathrm{sd}} \rangle - 0.569$, $U^{\mathrm{sd-sd}} = -2.90$ and $U^{\mathrm{c}} = -1.51$ for $M = 10$.

In Fig. 4, we show the dependence of the average minimum energy on M. The measured values of the minimum of $U^{\mathrm{sd-sd}}$ and U^{c} agree well with these results as a function of M. The variances of both $U^{\mathrm{sd-sd}}$ and U^{c} are exactly one and averages are zero when computed over the entire ensemble of the parameters in the generalized NK model. In each instance of the model, however, the average is not exactly zero, and the variance is not one. The term $U^{\mathrm{sd-sd}}$ is roughly Gaussian in each instance of the ensemble, since many individual interactions contribute to this term. The term U^{c} has a nonzero average in each instance of the ensemble, and this term is less nearly Gaussian, since fewer interactions contribute to this term.

[a] $\sigma_1^2 = 0.03084$, $\sigma_2^2 = 0.8404$, and $\sigma_3^2 = 0.4879$.

After VDJ recombination, the local optimization of these starting antibody sequences occurs by somatic hypermutation. Somatic hypermutation occurs at the rate of roughly one mutation per variable region of light and heavy chains per cell division, which occurs every 6 to 8 hours during intense cell proliferation.[42] Hence, in our simulation, we do 0.5 point mutations per sequence, keep the best (highest affinity) $x = 20\%$ sequences, and then amplify these back up to a total of 10^3 copies in one round, which corresponds to 1/3 day. That is, the probability of picking one of the, possibly mutated, sequences for the next round is $p_{\rm select} = 1/200$ for $U \leq U_{200}$ and $p_{\rm select} = 0$ for $U > U_{200}$, where U_{200} is the 200th best energy of the 10^3 sequences after the mutation events, and this equation is employed 10^3 times to select randomly the 10^3 sequences for the next round. Given a specific antigen, i.e. a specific set of interaction parameters, we conduct 30 rounds (10 days) of point mutation and selection in one immune response. In this way, memory B cells for the antigen are generated.

We can also calculate the lower bound for $U^{\rm sd-sd}$ after the 30 rounds of dynamics by neglecting the frustrations between the different $U_{ijk}^{\rm sd-sd}$ terms and assuming each term $U_{ijk}^{\rm sd-sd}$ is independently optimized. Each term has an effective population size of $Q^K = 625$. Since each σ_{ij}^k is Gaussian with zero mean and unit variance, we obtain the fully optimized bound

$$\langle U_{\rm min}^{\rm sd-sd} \rangle = \sqrt{\frac{DM(M-1)}{2}} \langle \min(x_i; i = 1, 625) \rangle = -51.00\,, \tag{13}$$

where $D = 6$ and $M = 10$. Frustration merely reduces the effective population size below Q^K, and so this bound is rigorous. A similar argument gives a lower bound for $U^{\rm c}$ as

$$\langle U_{\rm min}^{\rm c} \rangle = \sqrt{P} \langle \min(x_i; i = 1, 5) \rangle = -2.60\,, \tag{14}$$

with $P = 5$. A similar argument gives a lower bound for $U^{\rm sd}$ as

$$\langle U_{\rm min}^{\rm sd} \rangle = \sqrt{M(N-K+1)} \langle \min(x_i; i = 1, 625) \rangle = -25.97\,, \tag{15}$$

where $M = 10$, $N = 10$, and $K = 4$.

We calculate the affinity constant, introduced in Eq. (1), as a function of energy,

$$K^{\rm eq} = \exp(a - b\langle U \rangle)\,, \tag{16}$$

where a and b are determined by the dynamics of the mutation and selection process, $\langle U \rangle$ is the averaged best energy among many instances. Affinity constants resulting from VDJ recombination are roughly 10^4 l/mol, affinity constants after the first response of affinity maturation are roughly 10^6 l/mol, and affinity constants after a second response of affinity maturation are roughly 10^7 l/mol.[15] By comparison to the dynamics of the model, we obtain $a = -18.56, b = 1.67$, and $x = 20\%$.

4. Original Antigenic Sin

A consequence of the immune system response to antigen is the establishment of a state of memory.[43] Immunological memory gives the immune system the ability to respond more rapidly and effectively to antigens that have been encountered previously. Specific memory is maintained in the DNA of long-lived memory B cells that can persist without residual antigen.[44,45] Although our immune system is highly effective, some limitations have been reported. The phenomenon known as "original antigenic sin" is the tendency for antibodies produced in response to exposure to influenza virus antigens to suppress the creation of new, different antibodies in response to exposure to different versions of the flu.[46,47] Roughly speaking, the immune system responds only to the antigen fragments, or epitopes, that are in common with the original flu virus. As a result, individuals vaccinated against the flu may become *more* susceptible to infection by mutated strains of the flu than would individuals receiving no vaccination. The details of how original antigenic sin works, even at a qualitative level, are generally poorly understood.

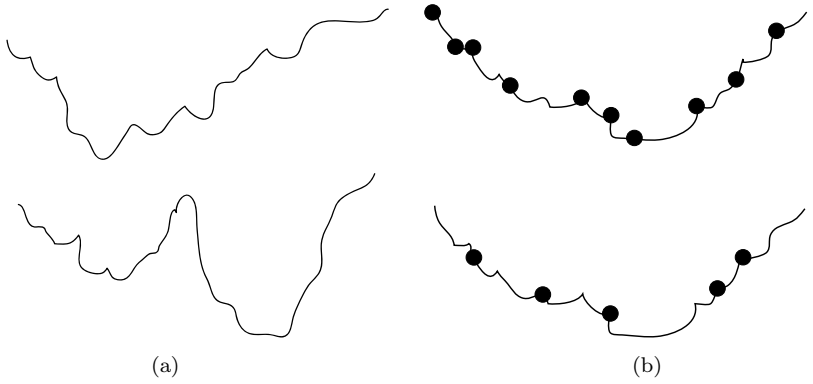

Fig. 5. (a) Localization in sequence space. The original energy landscape (top) corresponds to immune recognition of the original antigen. The immune recognition of a new antigen corresponds to a new energy landscape (bottom). The barrier between the antibody sequences favorable to the old and new antigens causes localization. (b) Reduction of diversity of antibody repertoire, represented by the black dots. More diversity on the top landscape and less on the bottom. The memory mechanism puts a restriction on the diversity and leads to original antigenic sin.

We describe the dynamics of affinity maturation by a search for increased binding constants between antibodies and antigen in antibody sequence space. There are two types of suboptimal dynamics that lead to original antigenic sin. One factor, shown in Fig. 5(a), is localization in sequence space. The sequence corresponding to the global minimum in the original energy landscape (original antigen), may correspond to a local minimum in the changed energy landscape (new antigen). This occurs because the antibodies that best recognize the original antigen are different from those that best recognize the new antigen. To get to the new global minimum, the immune system must overcome the barrier between the new global minimum

and the old global minimum, which is now a local minimum. The height and width of the barrier reflects the extent of the localization, and stronger localization causes slower dynamics and results in original antigenic sin. The other factor is the diversity of the initial sequences during the first response or the second response, shown in Fig. 5(b). A greater number of starting points, or more diversity, leads to a better chance of finding more favorable sequences during the local optimization. Each starting sequence finds a local minimum only, due to the local diffusion in sequence space that occurs in somatic hypermutation. An initial exposure produces memory sequences, which will be shown to reduce the diversity of subsequent responses. That is, the set of localized sequences produced in response to the first exposure reduces the ability of the immune system to respond to subsequent exposures to different, but related, antigens. Thus, it is the competitive process between memory sequences and naive B cells generated from VDJ recombination that is responsible for original antigenic sin in the immune system.

We estimate the number of memory and naive B cells that participate in a secondary immune response by the ratio of the respective affinity constants. From the definition of the affinity constant, $K^{\mathrm{eq}} = [\mathrm{Antigen} : \mathrm{Antibody}]/\{[\mathrm{Antigen}][\mathrm{Antibody}]\}$, the binding probability is proportional to the affinity constant and to the concentration of antigen-specific antibody, which is 10^2 times greater for the memory sequences.[15] We measure the average affinity of the 10^3 memory cells for the antigen in the secondary response, $K_{\mathrm{m}}^{\mathrm{eq}}$, and that of the 10^3 B cells from the naive repertoire of optimized subdomain sequences, $K_{\mathrm{n}}^{\mathrm{eq}}$. The ratio $10^2 K_{\mathrm{m}}^{\mathrm{eq}}/K_{\mathrm{n}}^{\mathrm{eq}}$ gives the ratio of memory cells to naive cells. For exposure to the second antigen, we perform 30 rounds (10 days) of point mutation and selection, starting with $10^5 K_{\mathrm{m}}^{\mathrm{eq}}/(10^2 K_{\mathrm{m}}^{\mathrm{eq}} + K_{\mathrm{n}}^{\mathrm{eq}})$ memory cells and $10^3 K_{\mathrm{n}}^{\mathrm{eq}}/(10^2 K_{\mathrm{m}}^{\mathrm{eq}} + K_{\mathrm{n}}^{\mathrm{eq}})$ naive cells, since both memory and naive sequences participate in the secondary response.[48] The dynamics of the first and secondary responses are shown in Fig. 6. The secondary dynamics can lead to better or worse affinities depending on how related the first and second antigen are, which is determined by the value of p.

Figure 7 shows the evolved affinity constant to a second antigen if the exposure to a first antigen exists (solid line) or not (dashed line) as a function of the difference between the first and second antigen, p, or "antigenic distance".[49] The distance, p, is given by the probability of changing parameters of interaction within the subdomain (U^{sd}), subdomain-subdomain ($U^{\mathrm{sd-sd}}$), and chemical binding (U^{c}) terms. Within U^{sd}, we change only the subdomain type, α_i, not the parameters σ_α, which are fixed by structural biology and should be independent of the antigen. All of these parameters change, not just those in U^{c}, because the antibody sequences that recognize an antigen change when the antigen changes. When the difference is small, exposure to a first antigen leads to a higher affinity constant than without exposure, which is why immune system memory and vaccination is normally effective. For a large difference, the antigen encountered in the first exposure is uncorrelated with that in the second exposure, and so immune system memory does not play a role. Interestingly, the immunological memory from the first exposure actually

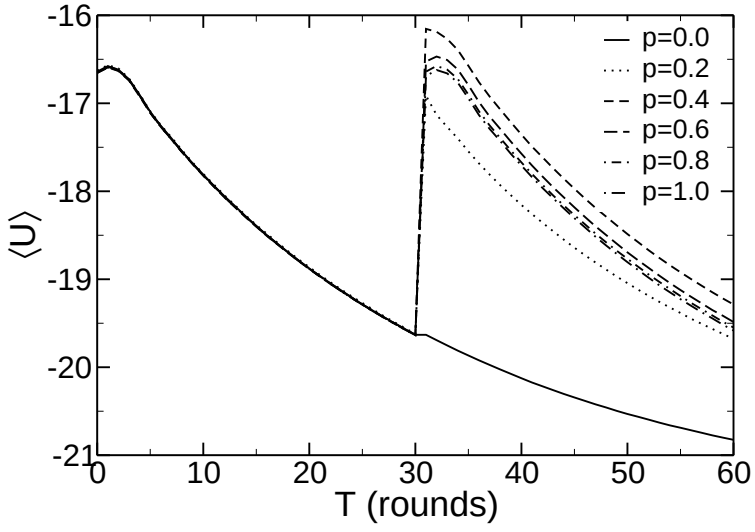

Fig. 6. The best binding energy averaged over 5000 instances as a function of time is shown. The first 30 rounds corresponds to the dynamics of the primary response to a certain antigen. At round 31, the antigen changes by fraction p, and the σ parameters in the generalized NK model change by probability p. The secondary response (the last 30 rounds) to the new antigen is a result of the competition between memory and naive sequences. In the case of $p = 0.4$, the secondary yields the worst energy corresponding to original antigenic sin.

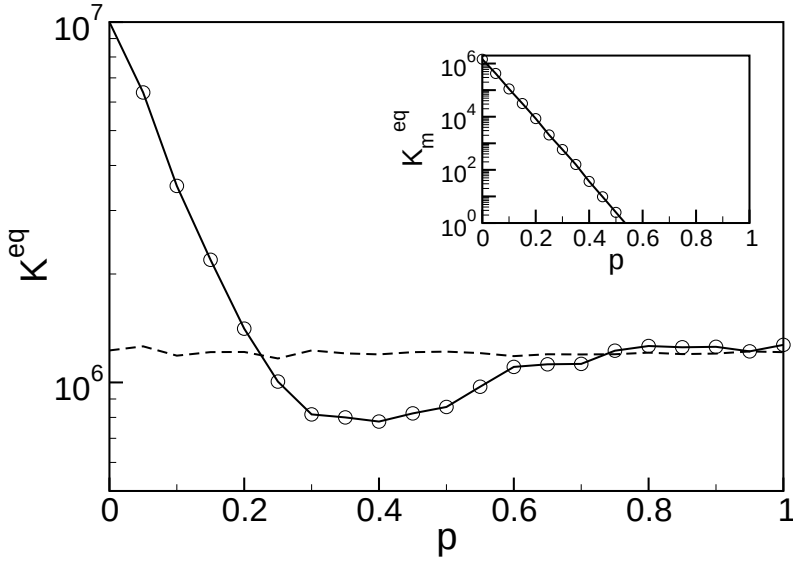

Fig. 7. The evolved affinity constant to a second antigen after exposure to an original antigen that differs by probability p (solid line). The dotted line represents the affinity constant without previous exposure. The affinity constant is generated by exponentiating, as in Eq. (16), the average of the best binding energy, using 5000 instances of the model. In inset is shown the affinity of the memory sequences for the mutated antigen.

gives worse protection, i.e. a lower affinity constant, for intermediate differences — which is original antigenic sin.

We also find that, as shown in the inset of Fig. 7, the affinity constant, K, decreases exponentially with the degree of antigenic change. That is, the binding energy, U, increases linearly with the change in the antigen, p. The linear behavior of the binding energy with p originates from each of the interaction parameters in the evolved energy being randomly changed to new ones with probability p. The fraction p of new σ values in $U^{\mathrm{sd-sd}}$ and U^{c} are centered around zero and negligible compared to the original, negative evolved values. In U^{sd}, a fraction p of the α_i are changed. Each changed subdomain has a probability of $1/5$ to change to the same type. The original, evolved sequence gives a value of roughly zero in a changed subdomain type α_j. The overall energy lost in U is, thus, proportional to p. Interestingly, the initial energy when $p = 1$ is $1/5$ of the initial energy when $p = 0$, or, $U(p = 1, T = 0) = U(p = 0, T = 0)/5$, where T is time or rounds of mutations. The reason for this result in that at $p = 1$ the only correlation is that α_i remains unchanged 20% of the time.

Note that in the primary response, and in the secondary response for $p \geq 0.6$, the first step of mutation and selection gives higher energy. Intuition tells us that the energy should decrease since we always select the 20% best sequences. The reason for the up tick lies in the correlation between mutation, selection, and the variance of the $N_{\mathrm{size}} = 1000$ of sequences. At each round, mutation itself will on average increase the energy of a sequence by $\langle \Delta \rangle \approx 0.3$, as shown in Fig. 8. The terms $U^{\mathrm{sd-sd}}$ and U^{c} are both lightly optimized initially and U^{sd} is heavily optimized initially, so a random mutation will lead to a worse energy with high probability. Normally, the variance of the sequences is comparable with $\langle \Delta \rangle$, so the selection of best 20% puts a selective pressure on all the sequences, including the best sequence, and selection leads to a lower energy. However, in the first round, the variance is about 3, much larger than $\langle \Delta \rangle$, and so the selection has no pressure on the mutated sequences arising from the best sequence, from which the sequences for the next round arise. So, in this first round, the best energy rises slightly.

Figure 8 shows $\langle \Delta \rangle$, the difference between the average binding energy before and after mutation as a function of time. The value of $\langle \Delta \rangle$ reflects the local barrier for mutations. In the primary response, $\langle \Delta \rangle$ increases with time, because as the binding energy becomes better, the probability to mutate to a worse sequence increases. In the secondary response, $\langle \Delta \rangle$ also increases with time for the same reason. Whether $\langle \Delta \rangle$ at the start of the secondary response is larger or smaller than the value at the start of the primary response depends on how different the new antigen is, i.e. the value of p. When p is small, the original sequences are somewhat optimized even for the new antigen, and so $\langle \Delta \rangle$ is larger in the secondary, compared to the primary, response. When p is large, the original sequences are unused for the new antigen, and so $\langle \Delta \rangle$ is the same in the secondary and primary responses. For intermediate values of p, when original antigenic sin occurs, the original sequences are maladapted and used for the new antigen, and so $\langle \Delta \rangle$ is smaller in the secondary than the primary response.

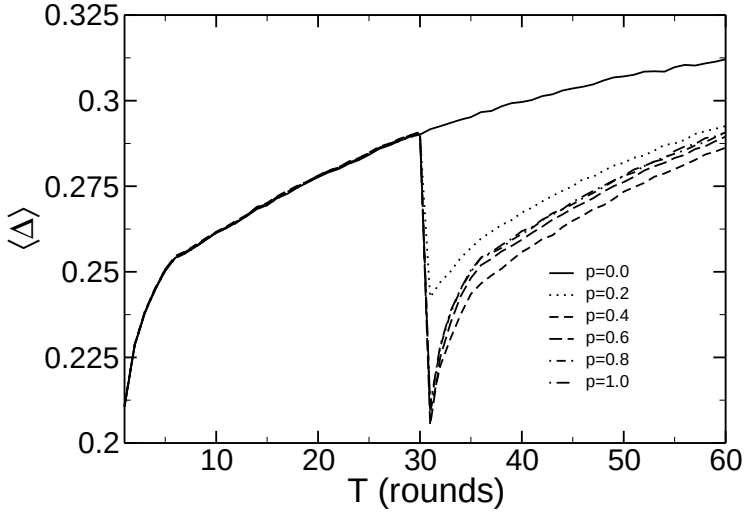

Fig. 8. $\langle\Delta\rangle$ as a function of time (rounds). The first 30 rounds correspond to the primary response, and the last 30 rounds correspond to the secondary response to a new antigen that differs from the first by fraction p. The value of Δ is the difference between the average binding energy of all sequences before and after mutation, but before selection, at each round. The results are averaged over 5000 instances.

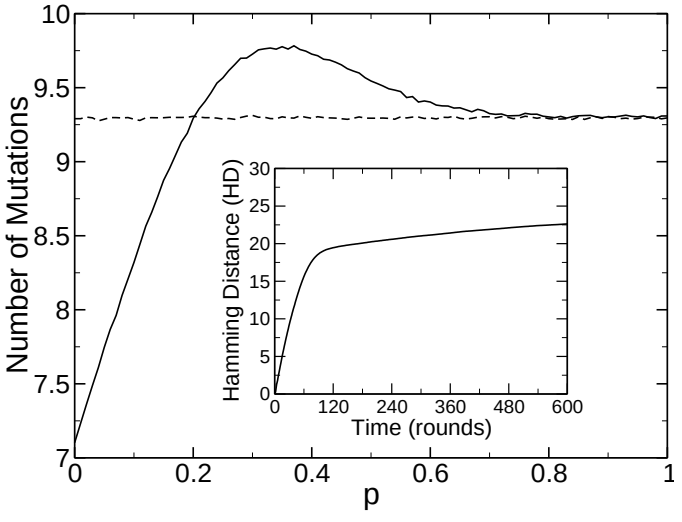

Fig. 9. The number of mutations in a secondary response after exposure to an original antigen that differs by probability p (solid line). The dotted line represents the mutations in the primary response, without previous exposure. The number of mutations is averaged over 50 000 instances of the model, and it is measured as the distance between the best evolved sequence and its ancestor.

In Fig. 9, we show that in the primary response, the average number of mutations after 30 rounds is about 9.3. The average number of mutations in the secondary response is less than 9.3 when $p < 0.20$, because the sequences are still somewhat

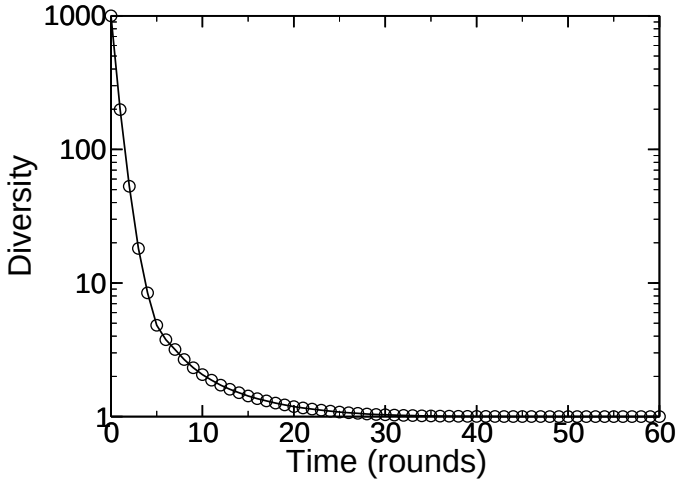

Fig. 10. Ancestral diversity as a function of time (rounds). Ancestral diversity is defined as the number of ancestors from which the sequences are derived. Results are averaged over 5000 instances of the model.

suitable for the modified antigen. The average number of mutations in the secondary response is more than 9.3 in the region $0.20 < p < 0.70$, which is approximately the region where original antigenic sin occurs. Localization causes more mutations to occur during the secondary response in the original antigenic sin region. That is, when p is small, the energy landscapes of the primary response and secondary response are similar, and the optimized sequences of the primary response are further optimized, although the dynamics is slowing down, and so there are fewer mutations in the secondary response. When p is sufficiently large, in the original antigenic sin region, the two landscapes are appreciably different. An optimal basin in the primary response may become a mediocre one or even a local minimum in the secondary response. Thus, additional mutations are required to escape from this region during the secondary response. This localization, or increased number of mutations during the secondary response, means that at least part of the barrier is entropic in nature. When the antigenic distance is even larger, $p > 0.7$, the two energy landscapes have little correlation, and the number of mutations is the same in the primary and secondary dynamics. Shown in the inset is the time evolution of the Hamming distance in the primary response. Hamming distance is defined as the number of amino acid differences between the best evolved sequence and its ancestor. We see dynamics of the Hamming distance observable slows at around 100 rounds signaling trapping in a local basin.

In Fig. 10, we show how the ancestral diversity, i.e. the number of ancestors from which the current round of sequences are derived, decreases with time. Ancestral diversity is naturally reduced in an exponential way by the selection that occurs during clonal expansion. While somatic hypermutation increases the sequence diversity, the ancestral diversity is unchanged by this process. At each round, the

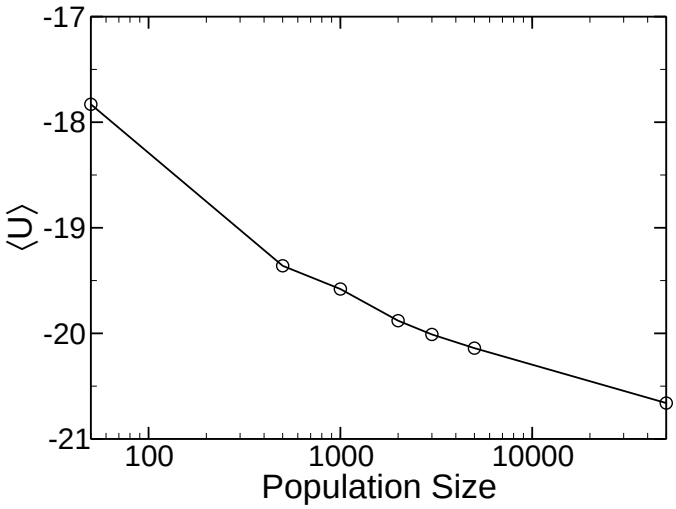

Fig. 11. The evolved energy after 30 rounds as a function of the population size of the sequences used in the simulation. The energy is the best evolved energy averaged over 5000 instances of the model.

top 20% of sequences are chosen, so mean field theory would predict the ancestral diversity to follow $f_{\text{diversity}} = 1000 \cdot \frac{1}{5}^t$, when $t \leq t_c$, $t_c = \frac{3 \ln 10}{\ln 5}$, and $f_{\text{diversity}} = 1$ otherwise. The results of the immune dynamics are not so simply described, showing the importance of a detailed, sequence-based model. By round 30, essentially all the sequences come from one ancestor with high probability. One implication is that the quality of initial VDJ recombinants is important, because at the end of the primary response, mutated versions of only one ancestral sequence survive. The final diversity is thus a small cloud of points around one of the initial sequences.

The final binding energy depends on the initial population size of the sequences in an approximately logarithmic manner, as shown in Fig. 11. Thus, by Eq. (16) the affinity constant has an approximately power law dependence on the population size. This power law arises solely due to the glassy dynamics of the evolution in sequence space. A diversity that is too small will lead to responses without sufficient resolution to identify suitable antibodies. Conversely, a diversity that is too large will waste biological resources. This power law dependence is an interesting result from our model and worthy of further study in experiments.

5. A New Order Parameter to Describe Antigenic Distance

To relate quantitatively the theory of Fig. 7 to influenza vaccine efficacy one must determine how the parameter p corresponds to antigenic distance. Immunoassays and crystallographic data show that only the epitope regions on the hemagglutinin protein of influenza A are significantly involved in immune recognition.[50] Thus, it is natural to assume that p is related to differences in the epitope regions only. We

introduce p_{epitope}, where

$$p_{\text{epitope}} = \frac{\text{number of amino acid differences in the dominant epitope}}{\text{total number of amino acids in the dominant epitope}} . \quad (17)$$

The dominant epitope is the epitope that induces the most significant immune response. It can be measured by competitive binding assays. For comparison to epidemiological data, we define the dominant epitope in a particular circulating virus strain as the epitope that has the largest fractional change in amino acid sequence relative to the vaccine strain for that particular year.[8,51–54] As our theory models the response of an immune system not subject to immunosenescence, we limited consideration to experimental studies of vaccine efficacy for 18 to 64 year old subjects in all years since sequencing began, when the H3N2 subtype of influenza A was the predominant virus, and where epidemiological data on vaccine efficacy exists. We focus on H3N2 subtype because it is the most common subtype, is responsible for significant morbidity and mortality, and has an abundance of available crystallographic, genetic, and epidemiological data. Our approach, however, is general.

We test p_{epitope} and the theory of Fig. 7 on all available epidemiological data for H3N2 vaccine efficacy in people. To apply the theory to a candidate vaccine and circulating strain, the sequences and identity of the dominant epitope must be known. The sequences and identities of the vaccine and circulating strains for each year were taken from Ref. 55. The definition of the five epitopes, or surface regions that are recognized by human antibodies, in the H3N2 hemagglutinin protein were also taken from Ref. 55. We determine the vaccine efficacy, E, from epidemiological studies in the literature,[56–70] where $E = (u - v)/u$, and u and v are the influenza-like illness rate of unvaccinated and vaccinated individuals, respectively. Thus, if the vaccine provides perfect protection against influenza in any one year then $E = 1.0$. A vaccine that is useless leads to $E = 0$. A vaccine that makes individuals more susceptible to influenza (i.e. original antigenic sin), leads to $E < 0$.

The difference between a vaccine strain and a circulating strain is defined in the model by p_{epitope}, Eq. (17). The vaccine efficacy, E, was assumed to correlate with the binding constant as $E = \alpha \ln[K_{\text{secondary}}(p_{\text{epitope}})/K_{\text{primary}}]$, where the constant α is chosen so that a perfect match between the vaccine and circulating strain leads to the average historical value of 45% vaccine efficacy, K_{primary} is the binding constant for the primary immune response, and $K_{\text{secondary}}$ is the binding constant for the secondary immune response following vaccination. The theory is entirely predictive, with no fitted parameters save for the determined constant α. For example, the point at which the vaccine efficacy becomes negative is independent of the value of α.

Shown in Fig. 12 are the epidemiologically determined vaccine efficacies and the efficacies predicted by the theory as a function of p_{epitope}. The statistical mechanical model captures the essential physics of the immune response to influenza vaccination and demonstrates the value of using p_{epitope} to define the degree of antigenic drift.

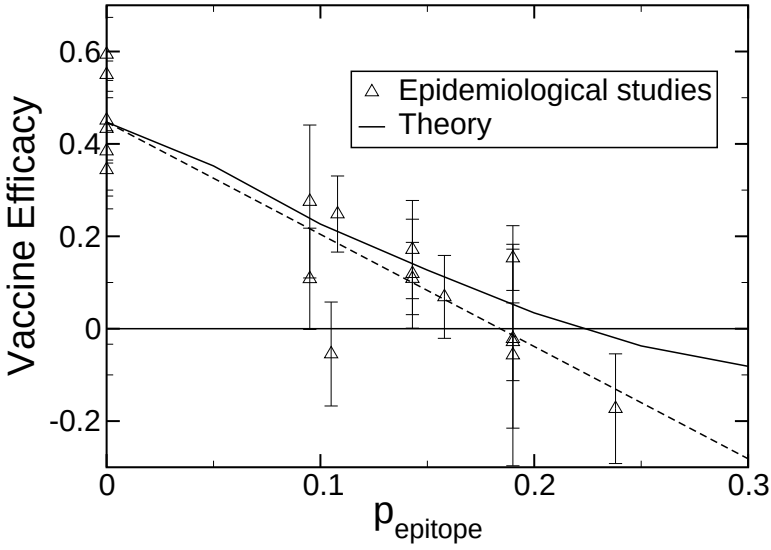

Fig. 12. Vaccine efficacy for influenza-like illness as a function of p_{epitope} as observed in epidemiological studies and as predicted by our theory. Also shown is a linear least squares fit to the data (long dashed, $R^2 = 0.81$). [Used with permission from [8], copyright 2006 Elsevier Ltd.]

When the antigenic drift, p_{epitope}, in the dominant epitope is greater than 0.19, according to historical epidemiological data, or 0.22, according to theory, the vaccine efficacy becomes negative (see Fig. 12). Error bars are calculated assuming binomial statistics for each data set: $\varepsilon^2 = [\sigma_v^2/u^2/N_v + (v/u^2)^2\sigma_u^2/N_u]$, where $\sigma_v^2 = v(1-v)$ and $\sigma_u^2 = u(1-u)$. If two sets of data are averaged in one year, then $\varepsilon^2 = \varepsilon_1^2/4 + \varepsilon_2^2/4$.

Methods currently employed by the World Health Organization (and the Centers for Disease Control in the U.S.) to quantify antigenic distance include calculating the sequence difference in the entire hemagglutinin protein,

$$p_{\text{sequence}} = \frac{\text{number of amino acid differences in the sequence}}{\text{total number of amino acids in the sequence}}\,, \tag{18}$$

and ferret antisera inhibition assays.[49,71] Plotting vaccine efficacy against the currently used methods (see Figs. 13 and 14) demonstrates that p_{epitope} correlates better with existing epidemiological data than the existing methods.

It would be logical to expect that the parameter p_{epitope} could be improved by the addition of more variables in the measure. We have developed a number of potential improvements to the original p_{epitope}. For example, one can include the influence of subdominant epitopes. One can make a distinction between conservative and non-conservative amino acid differences. One can consider the impact of amino acid differences at sites neighboring the epitope regions. And one can consider the significance of antigenic drift in the neuraminidase protein. None of these new measures has a significantly better correlation with the epidemiological efficacy

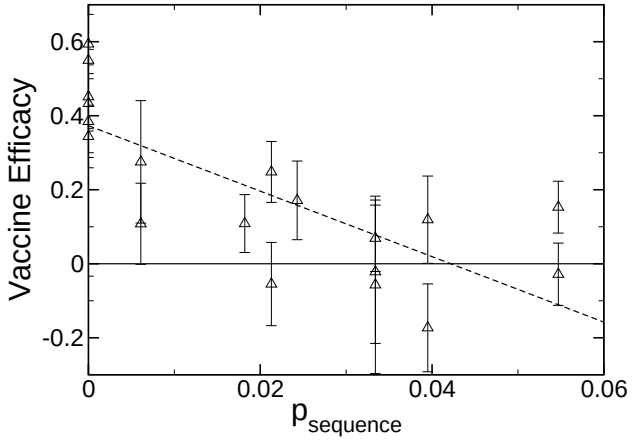

Fig. 13. Vaccine efficacy as observed in epidemiological studies for influenza-like illness as a function of p_{sequence} (see Eq. (18)). Also shown is a linear least squares fit to the data (long dashed, $R^2 = 0.59$). The epidemiological data shown in this figure are the same as in Fig. 12. Only the definition of the x-axis is different. [Used with permission from [8], copyright 2006 Elsevier Ltd.]

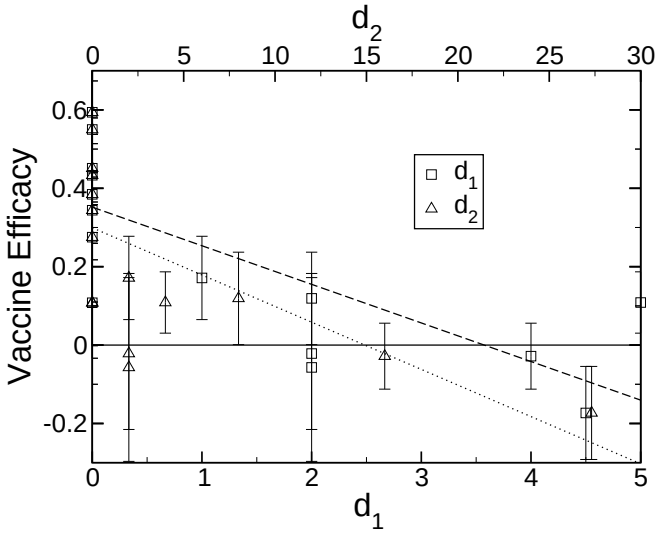

Fig. 14. Vaccine efficacy for influenza-like illness as a function of two measures of antigenic distance, d_1 (Ref. 49) and d_2,[71] derived from ferret antisera experiments. Experimental data were collected from a variety of sources.[49,72–77,b] Results were averaged when multiple hemagglutination inhibition (HI) studies had been performed for a given year. These HI binding assays measure the ability of ferret antisera to block the agglutination of red blood cells by influenza viruses. Also shown are linear least squares fits to the d_1 (long dashed, $R^2 = 0.57$) and d_2 (short dashed, $R^2 = 0.43$) data. The epidemiological data shown in this figure are the same as in Fig. 12. Only the definition of the x-axis is different. [Used with permission from [8], copyright 2006 Elsevier Ltd.]

[b]Information for FDA vaccine advisory panel meeting (1997), Centers for Disease Control, Atlanta, GA.

data available to us to date. Perhaps with the addition of more human vaccine efficacy data, some of these measures will provide an improvement over p_{epitope}.

6. Glassy Dynamics Suppresses Autoimmune Disease

Autoimmune disease occurs when an immune response is mistakenly directed at self antigens.[15] In most cases, the antibody/antigen interaction is highly specific. Sometimes, however, the antibody evolved in response to one antigen can bind to other antigens, and this phenomenon is called cross-reactivity.[78] Cross-reactivity occurs when another antigen has chemical features in common with the original antigen. Cross-reactivity is quantified experimentally by measuring the affinity of the antibody for the other antigen. Cross-reactivity is one mechanism by which autoimmune disease may develop. Individual susceptibility to autoimmune diseases has both a genetic and environmental basis. Multiple tolerance mechanisms at several biological levels normally act to reduce the probability of autoimmune disease.

In this section, we present two major results.[17] First, we show how different evolutionary mechanisms influence the relaxation dynamics of an evolving population of proteins. Specifically we study the dynamics of antibody generation by the immune system in response to pathogen invasion. These dynamics are crucial to the efficacy of the immune response. The immune system, as any biological system, has to respond in time to the threat, so the dynamics are crucial to the efficacy of the response. The hierarchical structure of our model protein Hamiltonian plays a critical role in the dynamics. The hierarchical structure also distinguishes our model from traditional short- or long-range spin glass energy models.[21,22] Second, we show that antibodies with significantly higher affinities to antigen than those produced in a primary immune response can be found with a biologically-plausible evolution process, but are more cross-reactive and would greatly increase susceptibility to autoimmune disorders. The concept of cross-reactivity is related to that of the chaos exponent in traditional spin glasses,[79,80] except that for cross-reactivity we are interested in the immediate energy response rather than in the equilibrated response of the system to a change in the couplings. Taking our two results together, we show that in the primary adaptive immune response a careful balance has evolved between specificity for and binding affinity to foreign antigen.

In our first study, we replicate the immune system dynamics. Each protein sequence is of the length of $N \times M = 100$ amino acids, corresponding to the length of the heavy chain variable region of an antibody. Initially there are 10^3 sequences, as in the human immune response.[16] Two different strategies are used in our simulations to search protein sequence space for high affinity antibodies. The first strategy mimics the normal adaptive humoral immune response. It starts with the combinatorial joining of optimized subdomains, after which the sequences undergo rounds of point mutation (PM) and selection as shown by the solid lines in Fig. 2. This is a simulation of the VDJ recombination, somatic hypermutation, and clonal selection that occurs in B cell development.[78] We generate five optimized

subdomain pools, each composed of 300 low-energy subdomains, corresponding to the $L = 5$ types. We use three sequences from each subdomain pool in our VDJ recombination, mimicking the known diversity.[16]

In our second study, we include a more powerful search of sequence space in the antibody evolution dynamics. VDJ recombination is used to generate an initial population, as in the normal immune response, but in addition to somatic hypermutation, we perform gene segment swapping (GSS) during each round of evolution and selection as shown by the dashed lines in Fig. 2. GSS-type processes are used by experimentalists to produce antibodies with binding constants $\approx 10^{11} - 10^{13}$ l/mol,[19] and exist within the natural hierarchy of evolutionary events.[11–14]

In the process of GSS, a subdomain belonging to one of the five types is replaced by another one from the optimized subdomain pool of the same type. Each sequence undergoes an average of 0.5 point mutations in each round of selection in both strategies. In GSS+PM, each subdomain in a sequence has a probability of 0.05 of being replaced in the process of GSS. Following mutation, selection occurs, and the 20% lowest energy antibodies are kept and are amplified to form the population of 10^3 sequences for the next round of mutation and selection. The primary response is comprised of 30 rounds of affinity maturation, corresponding to a lag phase of approximately 10 days,[16] during which B cells undergo clonal selection in response to antigen and differentiate into plasma cells and memory cells. The results that follow are averaged over 5000 instances of the ensemble.

The average affinity of the population of antibodies evolves during mutation and selection. The evolution of the binding energy under the two different strategies is shown in Fig. 15. The GSS+PM yields sequences with a lower energy than those

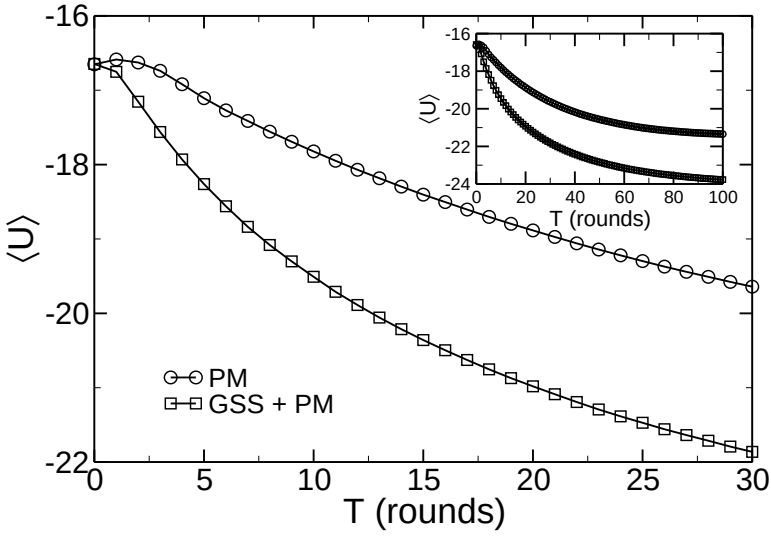

Fig. 15. Evolution of the affinity energy for the cases of point mutation (PM) only and gene segment swapping (GSS) plus PM as a function of the number of rounds of mutation and selection used to evolve the population of antibodies.

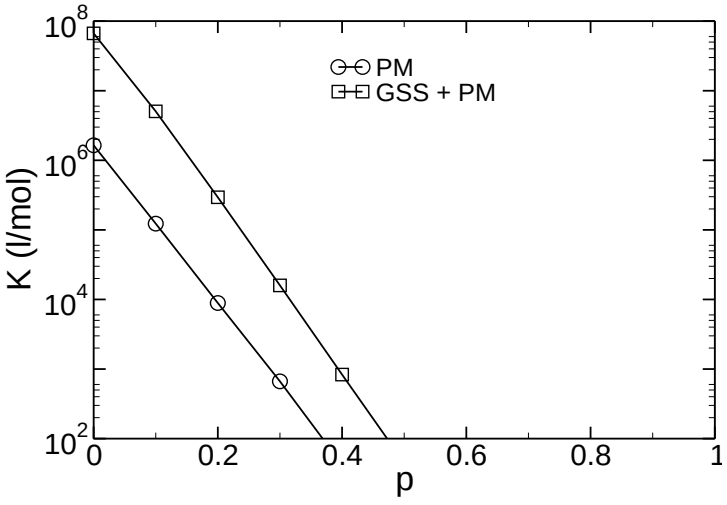

Fig. 16. Affinity of memory antibody sequences after a primary immune response for the two different immune system strategies (PM and GSS+PM) to altered antigens. The binding constant is K, and the antigenic distance of the new altered antigen from the original antigen is p. Cross-reactivity ceases at larger distances in the GSS+PM case ($p > p_2 = 0.472$) than in the PM only case ($p > p_1 = 0.368$).

from PM. The gap is due to each of the subdomains having an energy improved from an average to an exceptional one, $\Delta U \approx 10(U^{\rm sd}_{\rm best} - U^{\rm sd}_{\rm avg}) = -0.8$, and due to better sd-sd interactions found by GSS. In other words, the former is a better mechanism than the latter in searching sequence space for higher affinity antibodies to the given antigen. The best binding energy averaged over 5000 instances of the ensemble is -21.9 in the GSS+PM case and -19.7 in the PM only case at round 30, corresponding to affinities of $K = 6.7 \times 10^7$ l/mol and $K = 1.6 \times 10^6$ l/mol, respectively. So, GSS+PM yields an affinity more than an order of magnitude improved, which is even better than the affinity obtained from a secondary response by PM only.[16] That is, the multi-spin flips of GSS+PM especially accelerate the optimization of $U^{\rm sd-sd}$ in amino acid sequence space. Antibodies with a higher affinity to the antigen work more effectively in many ways. For example they can neutralize bacterial toxins, inhibit the infectiousness of viruses, and block the adhesion of bacteria to host cells at lower serum concentrations of antibody.[78] Based solely on Fig. 16, it is hard to understand why Darwinian evolution did not result in GSS+PM or any other more efficient strategy, rather than somatic hypermutation, as the preferred strategy for B cell expansion.

A calculation of cross-reactivity, which quantifies the specificity of the antibody, is used to compare the antibodies generated by the two strategies. Thirty rounds of primary response affinity maturation are conducted for both PM and GSS+PM. The antigen is then changed by p, and so each interaction parameter in the Hamiltonian is changed with probability p. The affinity constants are calculated for the new

antigen in the two cases. It is believed that when the affinity is less than 10^2 l/mol, the binding is not specific at all. So, we use $K > K_c = 10^2$ l/mol to tell when in each case, the cross-reactivity stops. As shown in Fig. 16, we find that cross-reactivity ceases at larger p in the GSS+PM case at $p_2 = 0.472$ than in the PM only case at $p_1 = 0.368$. So, cross-reactivity ceases when approximately $\Delta p = 0.10$ larger in the GSS+PM case. Within the region of specific binding, $K > 10^2$ l/mol, affinity is always better in the GSS+PM case. These cross-reactivity experiments show that the antibodies generated by the dynamics of GSS+PM can recognize more antigens and with higher affinity than those given by the PM dynamics only. Such cross reactivity has recently been observed.[81] The value of K decreases exponentially with the degree of antigenic change, p, for the same reasons as described to discuss the inset of Fig. 7.

Now the question we must answer is how many protein molecules are there between $p_1 = 0.368$ and $p_2 = 0.472$ that can be recognized by the antibodies produced through VDJ recombination and GSS+PM, but cannot be recognized by the antibodies produced through VDJ recombination and PM only. Antibodies recognize and bind to epitope regions of an antigen, so we are interested in how many epitopes these two different classes of antibodies are likely to recognize. We now show that the abnormal antibodies recognize 10^3 times more epitopes than do the antibodies produced by the normal primary immune response. We take the typical epitope length to be $B = 20$ amino acids.[78,82] In the theory, the antigenic distance is defined by the chemical composition of the epitope. The total number of possible epitopes is, therefore, 20^B since there are 20 different amino acids.[83] In Fig. 17 we show the normalized number of epitopes that are at an antigenic

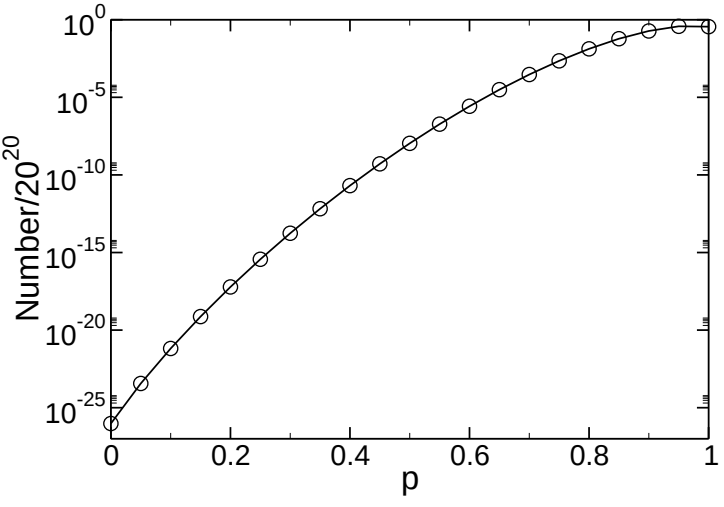

Fig. 17. The number of possible epitopes that are at an antigenic distance of p from another epitope. The epitopes are assumed to be 20 amino acids in length. The plot is normalized, so that $\sum_p N(p) = 20^{20}$.

distance of p from the native epitope of the antibody, given by

$$N(p) = 19^i B!/[i!(B-i)!], \tag{19}$$

where $i = pB$. This number is $N(p_1)/20^B = 2 \times 10^{-12}$ and $N(p_2)/20^B = 2 \times 10^{-9}$. The number of epitopes between $p = 0$ and p_1 and the number between p_1 and p_2 is approximately $A_1 \approx 2 \times 10^{-12}$ and $A_2 \approx 2 \times 10^{-9}$, respectively, since N grows exponentially with p. In the limit of large B,

$$\frac{N(p_2)}{N(p_1)} \sim \exp\{-B\{\ln[(1-p_2)/(1-p_1)] + p_1 \ln[19(1/p_1 - 1)] - p_2 \ln[19(1/p_2 - 1)]\}\}\,. \tag{20}$$

This ratio is 10^3 for 20 amino acids. The ratio varies between 160 and 4900 at the 15–25 amino acid limits of known epitope sizes. The ratio varies by only 30% with $\pm 10\%$ variation of both p values, within which the generalized NK model p values agree with experiment.[8,16]

In order to answer the question of why selection has favored the relatively slower dynamics in the immune response, we consider the function of the immune system as a whole rather than just the function of a single antibody binding to a single foreign antigen. The immune system is a delicate balance of a strong response to invading non-self antigens and weak or no response to self antigens. Thus, it is very important for the antibodies produced by the immune system to discriminate self from non-self.[84–86] An immune system incapable of recognizing an invading pathogen and initiating a response is an inadequate defense mechanism. On the other hand, production of antibodies binding to self antigens results in autoimmune diseases, e.g. diseases such as type I diabetes and rheumatoid arthritis.[15] It might be thought that GSS+PM would be superior dynamics, if only the immune system were able to perform ≈ 10 rounds. However, each subsequent exposure to related antigen would lead to another ≈ 10 rounds. After a couple such exposures, GSS+PM has evolved an unacceptably large binding constant, which saturates after several exposures to approximately 10^{10} l/mol, whereas PM saturates at the value of approximately 10^7 l/mol. The glassy dynamics of this evolution is shown in Fig. 18. The saturation of GSS+PM comes at a lower energy and at a later time than PM. This is why the former leads to autoimmunity.

Cross-reactivity can lead to autoimmune disease.[15] From Figs. 16 to 17, we know that the antibodies obtained at the end of a primary immune response can recognize a random epitope with a length of 20 amino acids with a probability of $\approx 10^{-12}$. It is also known that in a typical cell there are $\approx 10^4$ proteins, each with a length of ≈ 500 amino acids.[87] Antibodies binding to proteins recognize only surface epitopes. The amino acids exposed on the surface of proteins are typically part of a loop or turn, and typically 1/3 of the loop or turn is exposed. Thus, a typical contiguous recognition fragment length is 6–7 amino acids. Given a typical length of 20 amino acids for the entire loop or turn, and the typical epitope size of 20 amino acids, an antibody will recognize roughly 3 non-contiguous regions of length 6–7

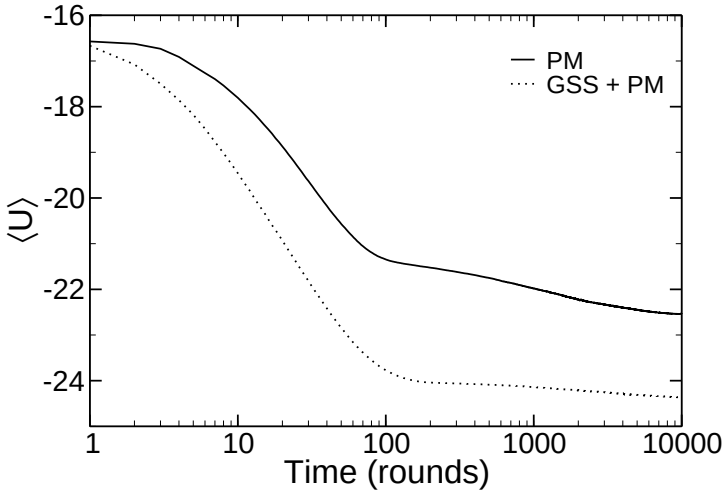

Fig. 18. Logarithmic, glassy dynamics in binding energy evolution for GSS+PM and PM. The slower logarithmic dynamics starts at around 80 in the PM case and around 100 in the GSS+PM case. The GSS+PM dynamics finds lower binding energies and is more likely to lead to autoimmunity.

amino acids in the protein sequence of 500 amino acids. There are approximately $500^3 \approx 10^8$ such epitopes. Given the 10^4 proteins in a cell, there will be $\approx 10^{12}$ total epitopes expressed in each cell. Thus, the number of epitopes recognized by a typical antibody in each cell is $A_1 \times 10^{12} \approx 1$. Even taking an exceptional protein of length 1000 amino acids, the number increases only to 10. Regulatory mechanisms can handle the occasional aberrant antibody, but cannot handle the 10^3 aberrant antibodies that GSS+PM would produce.

This remarkable result shows that the antibodies produced by the immune system recognize on average only their intended target. Conversely, antibodies that would be evolved in an immune response composed of VDJ recombination followed by a period of GSS+PM would recognize on average $A_2 \times 10^{12} \approx 10^3$ epitopes in each cell. Such antibodies, while having higher affinities for the intended target, would also lead to many more instances of autoimmune disease. Such promiscuous antibodies would place too large a burden on the regulatory mechanisms that eliminate the occasional aberrant antibody.[88] Thus, we find that selection has successfully evolved the human immune system to generate antibodies that recognize on average only the intended epitope after a humoral immune response. Inclusion of "more efficient" moves is generally excluded by the bound $A \times 10^{12} = O(1)$.

It is possible to test our prediction that proteins evolved with GSS+PM are more cross-reactive than proteins evolved with PM alone. Mechanisms such as DNA shuffling,[89] exon shuffling,[90,91] and swapping are like GSS. We predict that antibodies evolved with these methods will have higher figures of merit[20] as well as greater amounts of cross-reactivity. That is not to say that protein evolution cannot lead

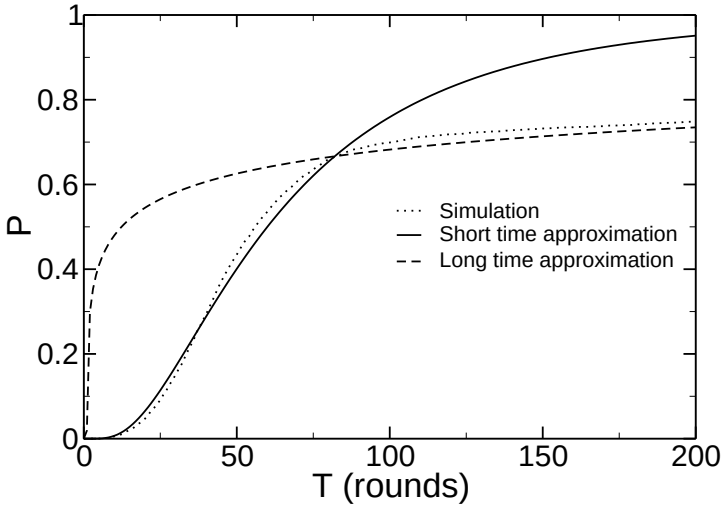

Fig. 19. Probability of inducing autoimmune disorder by a given time is shown for two different proposed immune system dynamics. The analytic results are also compared with simulation. The energy at round 60, $\langle U(60)\rangle$, corresponding to $K = 10^7$, is assumed to be the threshold of autoimmunity.

to increased specificity, but rather that on average increased antibody affinity will lead to increased cross-reactivity in the absence of other selective pressures.

Even with PM dynamics, our model predicts that chronic infection may lead to autoimmune disease, a mechanism postulated to be responsible for some fraction of autoimmune diseases,[92] including rheumatic diseases such as arthritis.[93] However, the strength and significance of this correlation is controversial.[94] Our model suggests a broad distribution for the time of onset of autoimmune disease due to chronic infection. Researchers have been looking for a clear, significant correlation in time, but a long distribution of onset times would lead to weaker statistical correlations, particularly in those cases where the infection persisted the longest. Searching for this distribution could elucidate this immunological puzzle and settle the scientific controversy.

To resolve the significance of this mechanism, we show in Fig. 19 the onset time distribution for autoimmunity. To do this, we assume that when the energy decreases below the natural value of $\langle U(60)\rangle$ arising from the PM-only dynamics, autoimmunity ensues. The natural value of $\langle U(60)\rangle$ corresponds to a binding constant of $K \simeq 10^7$ l/mol. To take into account randomness of the individual immune response, as well as the variation between different diseases, we assume that $U(30)$ follows a Gaussian distribution with variance of σ^2, where $3\sigma = b^{-1} \ln 10$, which corresponds to K in the range 10^5–10^7 l/mol for 99.5% of the instances of the ensemble. Based on Fig. 18, we take

$$U(T) = U(30) - c \cdot \ln\left(\frac{T}{30}\right) . \tag{21}$$

We decompose the curve into two regions and set c to be the slope of the segment between 30 and 70 in Fig. 18 in region one and the slope of the segment between 120 and 10000 in region two. Using only region one ignores glassy dynamics and assumes fast dynamics all the time. Using only region two neglects the fast dynamics before round 100 and assumes glassy dynamics all the time. Now, one can deduce the probability of reaching autoimmunity at time T due to the distribution of $U(30)$, because $p(T)dT = p[U(T)]dU(T)$,

$$p(T) = p[U(T)]\frac{dU(T)}{dT}\,. \tag{22}$$

Because of the monotonic nature of $U(T)$, the integration $P(T) = \int_0^T p(T)dT$ is the probability of having autoimmunity at time T. We know that the function from region one is reliable only for small T and the function from region two is valid for large T. Therefore, Fig. 19 gives the time distribution of autoimmunity. We see that a significant fraction of the autoimmunity, $\approx 30\%$, due to chronic infection occurs beyond the secondary dynamics region, even when we assume that the threshold for autoimmunity is the average binding constant at the end of the secondary dynamics.

We also measure in the generalized NK model simulation the percentage of instances with energy lower than $\langle U(60)\rangle$ at round T. This is a direct measure of the probability of inducing autoimmunity at a given time. We see that the analytic result is in good agreement with the measured one. We note that the generalized NK model as calibrated by Eq. (16) has variance about 15% less than that assumed above, and this is the reason for the discrepancy between the simulation and analytic theory at large times.

Thus, a mechanism which combines fast dynamics and glassy dynamics is chosen in the immune system to search amino acid sequence space. The glassy dynamics in PM itself inhibits autoimmunity by slowing down evolution at long times. It would be interesting to search for the onset time distribution in experiments, which would serve as one test for the existence of glassy dynamics in antibody evolution.

7. Conclusion

The immune system normally protects the human host against death by infection. We have introduced a hierarchical spin glass model of the evolutionary dynamics that occurs in the antibody-mediated immune response. Approximate analytical bounds on the terms within the model were derived. The model was used to provide a mechanism for original antigenic sin, wherein an initial exposure to antigen degrades the response of the immune system upon subsequent exposure to related, but different, antigens. These suboptimal dynamics were shown to result from a reduction in diversity of the responding antigens from a localization in sequence space of the evolving antibodies. A new order parameter to characterize antigenic distance was introduced. This order parameter correlates with efficacy of the influenza vaccine even better than results from animal model studies used by world health authorities. This order parameter would seem to be a valuable new tool for

making vaccine-related public health policy decisions. Finally, the glassy nature of evolution within the immune system was shown to play a functional role through inhibiting autoimmune disease. A balance has evolved in the mechanism for searching amino acid sequence space between affinity and specificity. That is, the normal immune response inhibits autoimmune disease at the cost of a weaker average binding affinity. It was suggested that the controversy related to the correlation between chronic infection and autoimmune disease might be addressed by searching for the predicted broad distribution of onset times for autoimmune disease.

References

1. World Health Organization Media Centre Influenza Fact Sheet 211 (2003), http://www.who.int/mediacentre/factsheets/fs211/en/.
2. J. R. Lave, C. J. Lin, M. J. Fine and P. Hughes-Cromick, *Sem. Respir. Crit. Care. Med.* **20** (1999) 189.
3. K. M. Neuzil, G. W. Reed, J. E. F. Mitchel and M. R. Griffin, *JAMA* **281** (1999) 901.
4. M. J. W. Sprenger, P. G. Mulder, W. E. P. Beyer, R. VanStrik and N. Masurel, *Int. J. Epidemiol.* **22** (1993) 334.
5. M. I. Meltzer, N. J. Cox and K. Fukuda, *Emerg. Infect. Dis.* **5** (1999) 659.
6. K. Stohr and M. Esveld, *Science* **306** (2004) 2195.
7. H. Varmus, R. Klausner, E. Zerhouni, T. Acharya, A. Daar and P. Singer, *Science* **302** (2003) 398.
8. V. Gupta, D. J. Earl and M. W. Deem (2005), q-bio.BM/0503030. Vaccine (2006), doi:10.1016/j.vaccine.2006.01.010.
9. Research Report – 2004-03-25, Press Releases, American Autoimmune Related Diseases Association, http://www.aarda.org/press_releases.php.
10. P. W. Anderson, *Proc. Natl. Acad. Sci. USA* **80** (1983) 3386.
11. J. A. Shapiro, *Genetica* **86** (1992) 99.
12. J. A. Shapiro, *Trends in Genetics* **13** (1997) 98.
13. D. J. Earl and M. W. Deem, *Proc. Natl. Acad. Sci. USA* **101** (2004) 11531.
14. M. G. Kidwell and D. R. Lisch, *Evolution* **55** (2001) 1.
15. C. A. Janeway, P. Travers, M. Walport and M. J. Shlomchik, *Immunobiology*, 6th edn. (Garland Publishing, New York, 2004).
16. M. W. Deem and H.-Y. Lee, *Phys. Rev. Lett.* **91** (2003) 068101.
17. J. Sun, D. J. Earl and M. W. Deem, *Phys. Rev. Lett.* **95** (2005) 148104.
18. G. M. Griffiths, C. Berek, M. Kaartinen and C. Milstein, *Nature* **312** (1984) 271.
19. R. Schier *et al.*, *J. Mol. Bio.* **263** (1996) 551.
20. L. D. Bogarad and M. W. Deem, *Proc. Natl. Acad. Sci. USA* **96** (1999) 2591.
21. K. H. Fischer and J. A. Hertz, *Spin Glasses* (Cambridge University Press, New York, 1991).
22. D. J. Gross and M. Mézard, *Nucl. Phys. B* **240** (1984) 431.
23. N. Bohr, *Nature* **137** (1936) 344.
24. T. Guhr, A. Müller-Groeling and H. A. Weidenmüller, *Phys. Rep.* **299** (1998) 189.
25. S. F. Edwards and P. W. Anderson, *J. Phys. F* **5** (1975) 965.
26. D. Sherrington and S. Kirkpatrick, *Phys. Rev. Lett.* **35** (1975) 1792.
27. B. Derrida, *Phys. Rev. Lett.* **45** (1980) 79.
28. G. Toulouse, *Commun. Phys.* **2** (1977) 115.
29. D. L. Stein and P. W. Anderson, *Proc. Natl. Acad. Sci. USA* **81** (1984) 1751.
30. J. D. Bryngelson and P. G. Wolynes, *Proc. Natl. Acad. Sci. USA* **84** (1987) 7524.

31. A. M. Gutin and E. I. Shakhnovich, *J. Chem. Phys.* **98** (1993) 8174.
32. B. Derrida and L. Peliti, *Bull. Math. Biol.* **53** (1991) 355.
33. S. Kauffman and S. Levin, *J. Theor. Biol.* **128** (1987) 11.
34. H. Kitano, *Nature Reviews* **5** (2004) 826.
35. G. Weisbuch, *J. Theor. Biol.* **143** (1990) 507.
36. B. Drossel, *Adv. Phys.* **50** (2001) 209.
37. A. S. Perelson and C. A. Macken, *Proc. Natl. Acad. Sci. USA* **92** (1995) 9657.
38. S. A. Kauffman and W. G. MacReady, *J. Theor. Biol.* **173** (1995) 427.
39. T. Tan, L. D. Bogarad and M. W. Deem, *J. Mol. Evol.* **59** (2004) 385.
40. G. M. Edelman, *Sci. Amer.* **223** (1970) 34.
41. R. R. Porter, *Science* **180** (1973) 713.
42. D. L. French, R. Laskov and M. D. Scharff, *Science* **244** (1989) 1152.
43. D. Gray, *Annu. Rev. Immu.* **11** (1993) 49.
44. F. L. Black and L. Rosen, *J. Immunol.* **88** (1962) 725.
45. J. Sprent, *Curr. Opin. Immunol.* **5** (1993) 433.
46. S. Fazekas de St. Groth and R. G. Webster, *J. Exp. Med.* **124** (1966) 331.
47. S. Fazekas de St. Groth and R. G. Webster, *J. Exp. Med.* **124** (1966) 347.
48. C. Berek and C. Milstein, *Immuno. Rev.* **96** (1987) 23.
49. D. J. Smith, S. Forrest, D. H. Ackley and A. S. Perelson, *Proc. Natl. Acad. Sci. USA* **96** (1999) 14001.
50. G. M. Air, M. C. Els, L. E. Brown, W. G. Laver and R. G. Webster, *Virology* **145** (1985) 237.
51. W. M. Fitch, J. M. Leiter, X. Li and P. Palese, *Proc. Natl. Acad. Sci. USA* **88** (1991) 4270.
52. R. M. Bush, C. A. Bender, K. Subbarao, N. J. Cox and W. M. Fitch, *Science* **286** (1999) 1921.
53. J. B. Plotkin and J. Dushoff, *Proc. Natl. Acad. Sci. USA* **100** (2003) 7152.
54. W. M. Fitch, R. M. Butch, C. A. Bender, K. Subbarao and N. J. Cox, *J. Heredity* **91** (2000) 183.
55. C. Macken, H. Lu, J. Goodman and L. Boykin, in *Options for the Control of Influenza IV*, eds. A. D. M. E. Osterhaus, N. Cox and A. W. Hampson, Hemagglutinin H3 epitope structural mapping (Elsevier Science, 2001), http://www.flu.lanl.gov/.
56. J. W. Smith and R. Pollard, *J. Hyg.* **83** (1979) 157.
57. W. A. Keitel, T. R. Cate and R. B. Couch, *Am. J. Epidemiol.* **127** (1988) 353.
58. W. A. Keitel, T. R. Cate, R. B. Couch, L. L. Huggins and K. R. Hess, *Vaccine* **15** (1997) 1114.
59. V. Demicheli, D. Rivetti, J. Deeks and T. Jefferson, *Cochrane Database Syst. Rev.* **3** (2004) CD001269.
60. K. M. Edwards, W. D. Dupont, M. K. Westrich, W. D. Plummer, Jr., P. S. Palmer and P. F. Wright, *J. Infect. Dis.* **169** (1994) 68.
61. D. S. Campbell and M. H. Rumley, *J. Occup. Environ. Med.* **39** (1997) 408.
62. K. L. Nichol, A. Lind, K. L. Margolis, M. Murdoch, R. McFadden, M. Hauge, S. Magnan and M. Drake, *N. Engl. J. Med.* **333** (1995) 889.
63. I. Grotto, Y. Mandel, M. S. Green, N. Varsano, M. Gdalevich, I. Ashkenazi and J. Shemer, *Clin. Infect. Dis.* **26** (1998) 913.
64. M. L. Clements, R. F. Betts, E. L. Tierney and B. R. Murphy, *J. Clin. Microbiol.* **23** (1986) 73.
65. C. B. Bridges, W. W. Thompson, M. I. Meltzer, G. R. Reeve, W. J. Talamonti, N. J. Cox, H. A. Lilac, H. Hall, A. Klimov and K. Fukuda, *J. Am. Med. Assoc.* **284** (2000) 1655.

66. M. A. Mixeu, G. N. Vespa, E. Forleo-Neto, J. Toniolo-Neto and P. M. Alves, *Aviat. Space Environ. Med.* **73** (2002) 876.
67. J. L. Millot, M. Aymard and A. Bardol, *Occup. Med.-Oxford* **52** (2002) 281.
68. N. Kawai, H. Ikematsu, N. Iwaki, I. Satoh, T. Kawashima, T. Tsuchimoto and S. Kashiwagi, *Vaccine* **21** (2003) 4507.
69. R. T. Lester, A. McGeer, G. Tomlinson and A. S. Detsky, *Infect. Cont. Hosp. Epidem.* **24** (2003) 839.
70. S. Dolan, A. C. Nyquist, D. Ondrejka, J. Todd, K. Gershman, J. Alexander, C. Bridges, J. Copeland, F. David, G. Euler *et al.*, *Centers for Disease Control and Prevention Morbidity and Mortality Weekly Report* **53** (2004) 8.
71. M. S. Lee and J. S. E. Chen, *Emerg. Infect. Dis.* **10** (2004) 1385.
72. N. Cox, A. Balish, L. Brammer, K. Fukuda, H. Hall, A. Klimov, S. Lindstrom, J. Mabry, G. Perez-Oronoz, A. Postema, *et al.*, in *Information for the Vaccines and Related Biological Products Advisory Committee, CBER, FDA, WHO Collaborating Center for Surveillance Epidemiology and Control of Influenza* (Centers for Disease Control, 2003).
73. G. W. Both, M. J. Sleigh, N. J. Cox and A. P. Kendal, *J. Virol.* **48** (1983) 52.
74. J. S. Ellis, P. Chakraverty and J. P. Clewley, *Arch. Virol.* **140** (1995) 1889.
75. M. T. Coiras, J. C. Aguilar, M. Galiano, S. Carlos, V. Gregory, Y. P. Lin, A. Hay and P. Perez-Brena, *Arch. Virol.* **146** (2001) 2133.
76. *WHO Weekly Epidemiological Record* **63** (1988) 57.
77. A. V. Pontoriero, E. G. Baumeister, A. M. Campos, V. L. Savy, Y. P. Lin and A. J. Hay, *Pan Am. J. Public Health* **9** (2001) 246.
78. R. A. Goldsby, T. J. Kindt, B. A. Osborne and J. Kuby, *Immunobiology*, 5th edn. (W. H. Freeman and Company, New York, 2002).
79. M. Ney-Nifle and A. P. Young, *J. Phys. A* **30** (1997) 5311.
80. V. Azcoiti, E. Follana and F. Ritort, *J. Phys. A* **28** (1995) 3863.
81. P. D. Holler, L. K. Chlewicki and D. M. Kranz, *Nature Im.* **4** (2003) 55.
82. E. T. Munoz and M. W. Deem, *Vaccine* **23** (2004) 1142.
83. N. A. Campbell and J. B. Reece, *Biology* 7th edn. (Benjamin Cummings, San Francisco, 2004).
84. J. K. Percus, O. E. Percus and A. S. Perelson, *Proc. Natl. Acad. Sci. USA* **90** (1993) 1691.
85. V. Detours, H. Bersini, J. Stewart and F. Varela, *J. Theor. Biol.* **170** (1994) 401.
86. J. Sulzer, L. van Hemmen, A. U. Newmann and U. Behn, *Bull. Math. Biol.* **55** (1993) 1133.
87. T. Tan, D. Frenkel, V. Gupta and M. W. Deem, *Physica A* **350** (2005) 52.
88. M. Larché and D. C. Wraith, *Nature Med.* **11** (2005) S69.
89. A. Crameri, S. A. Raillard, E. Bermudez and W. P. C. Stemmer, *Nature* **391** (1998) 288.
90. W. J. Netzer and F. U. Hartl, *Nature* **388** (1997) 343.
91. M. Ostermeier, J. H. Shim and S. J. Benkovic, *Nature Biotech.* **17** (1999) 1205.
92. D. Kaplan, I. Ferrari, P. L. Bergami, E. Mahler, G. Levitus, P. Chiale, J. Hoebeke, M. H. V. Van Regenmortel and M. J. Levin, *Proc. Natl. Acad. Sci. USA* **94** (1997) 10301.
93. M. Leirisalo-Repo, *Curr. Opin. in Rheumatology* **17**(2005) 433.
94. S. M. Carty, N. Snowden and A. J. Silman, *J. Rheumatology* **30** (2003) 425.